AGU ADVANCING EARTH AND SPACE SCIENCE

Geophysical Research Letters®

RESEARCH LETTER
10.1029/2021GL094115

Dynamics of Interannual Eddy Kinetic Energy Modulations in a Western Boundary Current

Junde Li[1], **Moninya Roughan**[1], **and Colette Kerry**[1]

[1]School of Mathematics and Statistics, Coastal and Regional Oceanography Lab, UNSW Sydney, Sydney, NSW, Australia

Key Points:

- Barotropic instabilities dominate eddy shedding and control variability of eddy kinetic energy (EKE) in the East Australian Current
- There is a clear (inverse) relationship between poleward transport at 28°S and the latitude that anticyclonic eddies are shed
- Transport at 28°S and sea level anomalies at ~27°S–29°S (upstream) are significantly correlated with EKE at ~33.1°S–36.6°S (downstream)

Supporting Information:

Supporting Information may be found in the online version of this article.

Correspondence to:

J. Li,
junde.li@unsw.edu.au

Citation:

Li, J., Roughan, M., & Kerry, C. (2021). Dynamics of interannual eddy kinetic energy modulations in a Western Boundary Current. *Geophysical Research Letters*, *48*, e2021GL094115. https://doi.org/10.1029/2021GL094115

Received 28 APR 2021
Accepted 18 SEP 2021

Abstract Among Western Boundary Currents, the East Australian Current (EAC) has a more energetic eddy field relative to its mean flow, however, the relationship between upstream transport and downstream eddy kinetic energy (EKE) is still unclear. We investigate the modulation of downstream EKE in the EAC's typical separation region (Tasman EKE Box) (33.1°S–36.6°S) based on a long-term (22-year), high-resolution (2.5–6 km) model simulation and satellite altimeter observations from 1994 to 2016. Our results show that the poleward EAC transport at 28°S leads the EKE in the Tasman EKE Box by 93–118 days. Barotropic instabilities are the primary source of EKE, and they control EKE variability in the EAC system. Anticyclonic eddies shed from the EAC dominate from 33°S–36°S during high-EKE periods, but in low-EKE periods anticyclonic eddies penetrate even further south by ~2°.

Plain Language Summary The East Australian Current (EAC) mean flow is typically coherent from ~27°S–32°S (upstream), but eddies form after it separates from the coast typically at ~32°S, associated with high eddy variability downstream. However, we know little about what drives changes in the downstream eddies and the correlation with transport upstream. Here, we use both satellite observations and model simulations to investigate the interannual variability in the eddy field. We find that the transport upstream of separation is well correlated with the variability of sea surface height within the typical EAC separation region. An anomalously higher EAC transport at 28°S corresponds to an anomalously higher sea surface height within the typical EAC separation region. The reverse is true when the EAC transport is weaker, but the current separates from the coast further to the south. We also show that the energy converted from the mean flow to the eddy fields is mainly through mean kinetic energy to eddy kinetic energy.

1. Introduction

1.1. Eddies in the East Australian Current System

The East Australian Current (EAC) is the energetic Western Boundary Current (WBC) of the South Pacific subtropical gyre. The EAC flows poleward along southeastern Australia, separates from the coast typically at around 32°S (Cetina-Heredia et al., 2014), bifurcating into the eastward flow toward New Zealand (EAC eastern extension) and the southward flow toward Tasmania (EAC southern extension). Here we follow the terms introduced by Oke et al. (2019), however, it is noted that the EAC eastern extension has been traditionally referred to as the Tasman Front, and the EAC southern extension has been traditionally referred to as the EAC extension. The EAC sheds large anticyclonic eddies with a timescale of 90–180 days at the separation point (Bowen et al., 2005), and cyclonic eddies often form during the shedding of the anticyclonic eddy, creating a typical counter-rotating eddy dipole structure (Malan et al., 2020). The EAC can separate at any latitude along its length (Cetina-Heredia et al., 2014; Oke et al., 2019), therefore eddies can originate as far north as 25°S (Qiu et al., 2014), with maximum intensity between 32°S and 35°S (Bowen et al., 2005). Eddy processes, including eddy generation, shedding and propagation, are accompanied by high eddy kinetic energy (EKE). The interannual variability of EKE has been detected in mesoscale eddy activity in most high EKE regions, including the Agulhas Current (Zhu et al., 2018) and the Kuroshio Current (Nonaka et al., 2020). In the EAC region, both 10-year satellite observations (Qiu & Chen, 2004) and 22-year high-resolution ocean model simulations (Kerry & Roughan, 2020) show that the EKE has a strong annual cycle. However, little is known about the mechanism causing the interannual variability of EKE in the EAC.

1.2. Energetics of Eddy-Mean Flow Interactions

WBCs and associated mesoscale eddies can exchange energy, vorticity and momentum through eddy-mean flow interactions (Chen et al., 2014; Greatbatch et al., 2010; Kang & Curchitser, 2015). The transfer of energy from the mean flow to eddies through barotropic and baroclinic instabilities leads to eddy formation and shedding (Macdonald et al., 2016). In turn, the energy transferred from the eddies back to the mean flow can feed the mean flow (Kuo & Chern, 2011; Mata et al., 2006). Energetics analysis is an effective method of quantifying the energy exchange between the mean flow and eddy reservoirs. It has been widely used to investigate dynamical processes of eddy activity and current variability in other WBCs, for example, in the Gulf Stream (Gula et al., 2015; Kang & Curchitser, 2015; Schubert et al., 2018), Kuroshio Current (Yan et al., 2019; Yang & Liang, 2016, 2018), Brazil Current (Magalhães et al., 2017), and Agulhas Current (Halo et al., 2014). Energetics analysis has also been conducted to investigate the EAC eddy shedding process. Bowen et al. (2005) propose that barotropic instabilities play a dominant role in driving an eddy shedding event. However, Mata et al. (2006) and Bull et al. (2017) suggest that both barotropic and baroclinic instabilities are responsible for eddy generation, with barotropic energy conversion dominating.

To improve our understanding of oceanic energetics of eddy-mean flow interactions, a minimum horizontal resolution of 10 km is required to represent both mesoscale variability and the WBC adequately (Chassignet & Xu, 2017; Maltrud & McClean, 2005; Storch et al., 2012). However, horizontal resolutions used previously for modeling energetics studies in the EAC region have been much coarser (>20 km). In addition, to the best of our knowledge, the energy conversion term representing the energy transfer from eddy available potential energy (EPE) to EKE has never been investigated in the EAC region despite many studies in other WBCs.

1.3. Transport in the East Australian Current System

Compared with other mid-latitude WBCs, the EAC has a weaker transport and mean flow due to the loss of transport from the South Equatorial Current into the Indonesian Throughflow (Godfrey, 1989). EAC transport has been estimated by combining XBT observations and satellite altimeter data (Ridgway et al., 2008; Zilberman et al., 2018), from mooring array data (Mata et al., 2000; Sloyan et al., 2016) and numerical simulations (Cetina-Heredia et al., 2014; Kerry et al., 2016, 2018; Kerry & Roughan, 2020; Ribbat et al., 2020; Ypma et al., 2016). Time series of these estimated EAC transports have shown a range of temporal signals from eddy shedding, seasonal, interannual to decadal timescales, particularly the strong interannual variability upstream of the typical separation point (Cetina-Heredia et al., 2014; Kerry & Roughan, 2020; Oke et al., 2019). Sloyan and O'Kane (2015) show that the EAC transport variability at 25°S is significantly anti-correlated to EAC southern extension transport (P-value <0.05, $R = -0.14$). Furthermore, Sloyan et al. (2016) suggest that the EAC variability in the Tasman Sea may be linked to variability upstream of 27°S. However, whether there is a statistically significant relationship between transport upstream of separation and downstream eddy activity remains unclear.

In this study, we use a long-term (22-year) satellite altimetry product and high-resolution (2.5–6 km) ocean model simulation to achieve three objectives. First, we investigate the interannual variability in EKE in the EAC System (Section 3.1). Second, we examine the energetics of eddy-mean flow interactions in the EAC System to reveal the dynamical mechanisms responsible for the interannual modulation of downstream EKE (Section 3.2). Lastly, we assess the relationship between the interannual variability of downstream EKE with transport upstream of separation and sea level anomaly (SLA) (Section 3.3).

2. Data and Methods

2.1. Satellite Observations

The daily satellite observations, including SLA, absolute geostrophic current velocity and geostrophic current velocity anomalies, are obtained from Archiving, Validation and Interpretation of Satellite Oceanographic (AVISO+) (Ducet et al., 2000). These data are suitable to study the mesoscale ocean variability in WBC regions (Halo et al., 2014; Zhu et al., 2018). The AVISO+ daily data used here spans an approximately

22-year period from 1994 to 2016, with a horizontal resolution of 1/4°. AVISO+ has shown its ability to capture the eddy activity in the EAC system, with similar eddy statistics between AVISO+ and the 1/10° ocean model (Oliver et al., 2015).

2.2. Numerical Simulations

The Regional Ocean Modeling System (ROMS) configuration of the EAC system used here is described in Kerry et al. (2016); Kerry and Roughan (2020). The model has a horizontal resolution of 2.5–6 km, which is suitable for resolving the mesoscale eddies in the EAC system (full details of the model configuration are in Text S1). The 22-year simulation in Kerry and Roughan (2020) uses atmospheric forcing from the National Center for Environmental Prediction's (NCEP) reanalysis, and they show that the mean and variability of the simulated ocean state compares well with observations. In this study, we use the same model configuration except that atmospheric forcing is provided from the hourly 12-km Bureau of Meteorology Atmospheric high-resolution Regional Reanalysis for Australia (BARRA-R) (Su et al., 2019). We also include the barotropic tidal constituents extracted from the TPXO8 global tidal model (Egbert & Erofeeva, 2002). The mean circulation and mesoscale variability are similar between the 22-year simulation of Kerry and Roughan (2020) and this simulation, providing confidence that this simulation provides an accurate representation of the EAC, its separation from the coast and its eddy field. Compared to NCEP, BARRA-R has more realistic heat fluxes close to the coast due to its higher resolution. The numerical simulation of the ocean circulation using BARRA-R atmospheric forcing has significantly reduced the cold sea surface temperature (SST) biases compared to satellite observations of SST. Further details of the model configuration (Li et al., 2021) and validation are in Text S2 and Figures S1–S3.

2.3. Energy Conversion Terms

Energetics analysis is used to quantify the depth-dependent mean kinetic energy (MKE), EKE, and energy conversion terms (Kang & Curchitser, 2015). To investigate the eddy-mean flow interactions in the EAC region, we calculate the following energetics metrics:

$$\mathrm{MKE} = \frac{1}{2}(\overline{u}^2 + \overline{v}^2) \tag{1}$$

$$\mathrm{EKE} = \frac{1}{2}(u'^2 + v'^2) \tag{2}$$

$$\mathrm{KmKe} = -\rho_0\left[\overline{u'u'}\frac{\partial \overline{u}}{\partial x} + \overline{u'v'}\frac{\partial \overline{u}}{\partial y} + \overline{v'u'}\frac{\partial \overline{v}}{\partial x} + \overline{v'v'}\frac{\partial \overline{v}}{\partial y}\right] \tag{3}$$

$$\mathrm{PeKe} = -g\overline{\rho' w'} \tag{4}$$

where $\overline{u}$ and $\overline{v}$ are the time-mean zonal and meridional velocities, respectively. u', v', w' are the perturbations in time of the zonal, the meridional and vertical components of the flow, respectively. ρ' is the perturbation of the background reference density $\rho(z)$. Following Kang and Curchitser (2015), we calculate $\rho(z)$ by averaging the density over time and area. The constant part of the reference density ρ_0 is 1,025 kg m^{-3}, and the acceleration due to gravity g is 9.81 m s^{-2}. The energy conversion term KmKe represents the energy transfer rate from MKE to EKE, and a positive value indicates the eddy formation through barotropic instabilities of the mean flow (Kang & Curchitser, 2015). The other energy conversion term PeKe represents the energy transfer from EPE to EKE due to the baroclinic instability (Halo et al., 2014). The energy transfer terms KmKe and PeKe are sources of EKE growth along mean streamlines of the flow (Schubert et al., 2018).

The observed MKE and EKE are estimated from AVISO geostrophic velocities. We also calculate the surface MKE and EKE from the model geostrophic currents based on $u = -\frac{g}{f}\frac{\partial \eta}{\partial y}$ and $v = \frac{g}{f}\frac{\partial \eta}{\partial x}$, where η is the sea level, f is the Coriolis parameter. We average the EKE, KmKe and PeKe over the upper 450 m to investigate the eddy-mean flow interactions from the model output. The upper 450 m was chosen here because the EKE is highest in this depth range (Kerry & Roughan, 2020; Kerry et al., 2018).

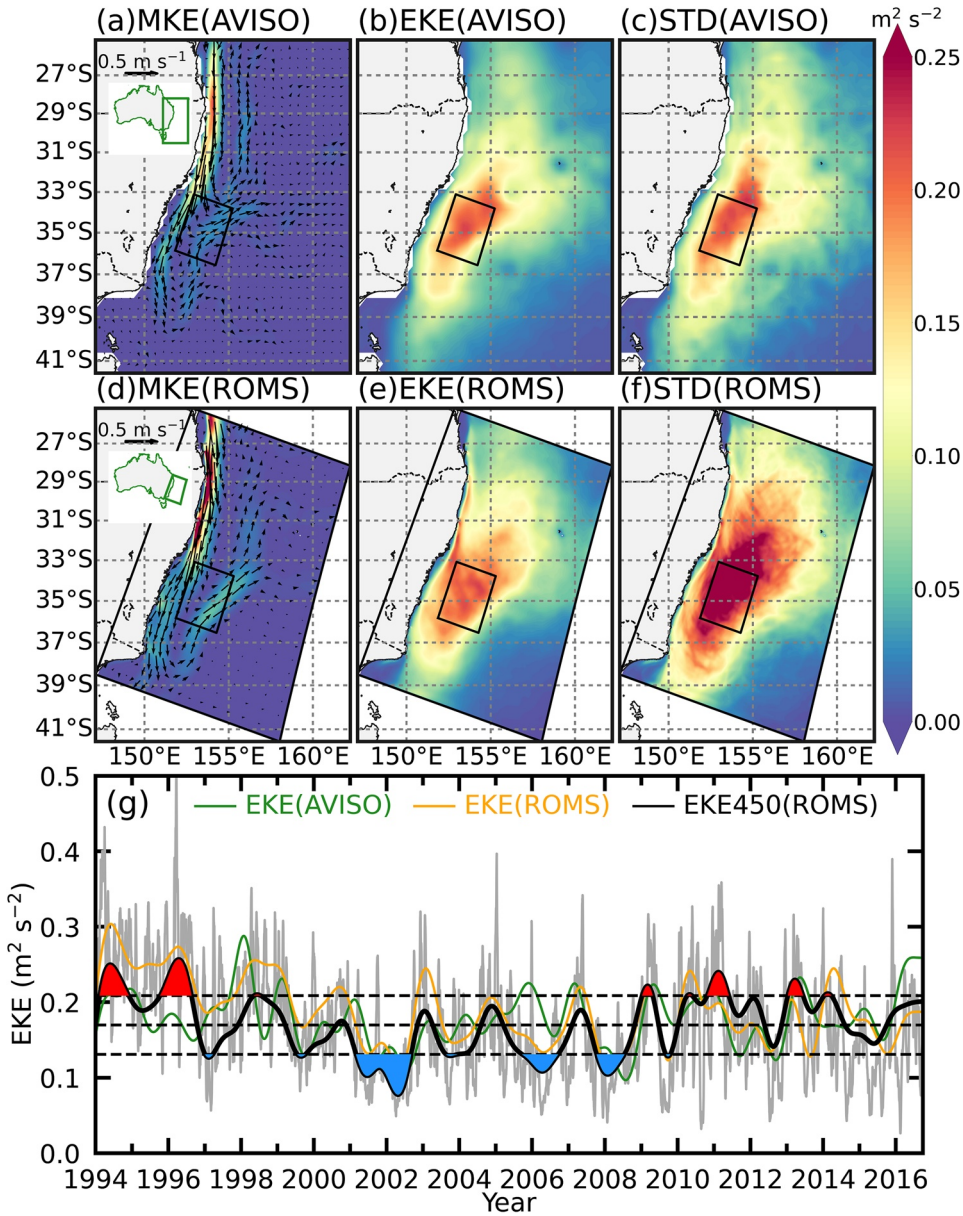

Figure 1. (a) Mean kinetic energy and mean surface geostrophic velocities (vectors) (b) mean eddy kinetic energy (EKE) and (c) Standard Deviation (STD) of the EKE derived from Archiving, Validation and Interpretation of Satellite Oceanographic (AVISO) geostrophic velocities and geostrophic velocity anomalies over the 22 years. (d–f) Same as (a–c), but calculated from the ROMS model geostrophic velocities and geostrophic velocity anomalies. The black box in (a–f) indicates the Tasman EKE Box (~33.1°S–36.6°S, ~151.8°E–155.2°E). (g) Time series of the 1-year low-pass filtered surface EKE from AVISO (green line), ROMS (orange line), and EKE450 from ROMS (black line) averaged within the Tasman EKE Box. The gray line denotes the raw time series with the linear trend removed. Periods when EKE450 is larger (smaller) than 1.0 STD are highlighted in red (blue).

3. Results

3.1. Interannual Variability of EKE

The EAC jet flows poleward coherently with a band of high surface MKE over the shelf between 27°S and 32°S (Figure 1a). Generally, the spatial distribution of MKE in ROMS is in good agreement with the AVISO observations (Figure 1d). MKE significantly reduces after the jet separates from the coast with low MKE in the EAC southern extension and a relatively small MKE band in the EAC return flow region. Large

anticyclonic eddies shed after the EAC jet separates from the coast, resulting in high EKE amplitude and variability. In this study, we focus on the EKE variability in the typical EAC separation region (black box in Figure 1, hereafter referred to as Tasman EKE Box), where the surface EKE is highest (Figures 1b and 1e), and the Standard Deviation (STD) of EKE also exhibits elevated EKE variability (Figures 1c and 1f).

To investigate the interannual variability in the high EKE region of the EAC system, we compute the spatially averaged EKE over the Tasman EKE Box from both AVISO and ROMS. Frequency spectra of the daily AVISO surface EKE, ROMS surface EKE and ROMS EKE averaged over the upper 450 m (EKE450) show strong peaks at the annual timescale, with high energy within a range of 270–500 days (Figure S4). ROMS has a small peak at around a 200-day period which is absent in AVISO, but the ~90-day peak in ROMS is shorter than that in AVISO. A 1-year low-pass Butterworth filter is further applied to the EKE time series to remove the signals shorter than the annual period (Figure S4). Generally, the low-frequency variability of the ROMS surface EKE agrees well with the AVISO surface EKE (Figure 1g). The linear correlation coefficient between the two time series reaches 0.50 (95% significance level). While we do not expect the mesoscale eddy field to evolve in the same way as the ocean state sampled by AVISO, the non-zero correlation may be due to the fact that the model is receiving boundary conditions and surface forcing from reanalysis products. The low-pass filtered time series of EKE450 (black line) is also highly correlated with the ROMS surface EKE, with a correlation coefficient of 0.96 (95% significance level). Despite the fact that there are some spectral differences in periods shorter than 1 year, the differences are not statistically significant at 95% confidence intervals (Figure S4), suggesting that the model represents the EKE's interannual variability and anomalies well.

We define high-EKE (low-EKE) periods when the EKE450 is larger (smaller) than the mean EKE450 plus (minus) one standard deviation of the EKE450 time series as in Sun et al. (2016) (Figure 1g). The mean EKE450 in ROMS averaged over the Tasman EKE Box during the high-EKE periods, the full 22-year period, and the low-EKE periods is 0.24 $m^2\ s^{-2}$, 0.17 $m^2\ s^{-2}$ and 0.11 $m^2\ s^{-2}$, respectively. Over the 22 years, the percentages of time defined as high-EKE periods and low-EKE periods are 15.3% and 18.1%, respectively. For comparison, we apply the same approach to the AVISO surface EKE and obtain similar percentages of 15.5% and 16.3% for the high-EKE and low-EKE periods in AVISO. By definition, both the high-EKE and low-EKE percentages in AVISO and ROMS are close to a normal distribution.

3.2. Energy Conversions

We use composite analysis to investigate the interannual modulation responsible for the large amplitude EKE anomalies using the ROMS model. Figure 2 shows the composite EKE450 anomalies, KmKe and PeKe averaged over the upper 450 m, SLA and surface southward velocity in the high-EKE and low-EKE periods. By definition, there are large positive EKE450 anomalies in the Tasman EKE Box during the high-EKE periods (Figure 2a) and anomalous low EKE450 within the Tasman EKE Box during the low-EKE periods (Figure 2f).

Consistent with previous studies (Bowen et al., 2005; Macdonald et al., 2016; Mata et al., 2006), barotropic instabilities dominate EKE variation in the Tasman EKE Box (Figure S5a). We find large positive (negative) KmKe anomalies during the high-EKE (low-EKE) periods (Figures S5b and S5c). North of the Tasman EKE Box, two strong positive KmKe bands are observed along the coast in both high-EKE (Figure 2b) and low-EKE periods (Figure 2g). One is located between 28°S and 30.5°S, and the other is between 31.5°S and 33.5°S. East of these two bands, the KmKe is also relatively strong. Positive KmKe indicates that eddies drain energy from the MKE to drive a shedding event. Our energetics analysis shows that eddies can gain energy from the mean flow at any latitude between 28°S and 33.5°S, with the strongest barotropic energy conversion at ~33.5°S. These results are consistent with the occurrence of EAC separation latitude in Kerry and Roughan (2020, Figures 2d–2e) and Cetina-Heredia et al. (2019, Figure 2c). The energy transfer timescale ($\rho_0 MKE/KmKe$) is shorter than 2 days in most regions of the Tasman EKE Box (Figures S5g–S5i), indicating that eddies can drain energy from the mean flow and shed in a short time in these regions. Strong positive KmKe occurring at the separation point reveals that barotropic instabilities of the mean flow result in the eddy shedding when EAC separates from the coast with large velocity perturbations. During the high-EKE periods, the EAC jet separates from the coast to the north of the Tasman EKE Box and flows eastward, shedding an anticyclonic eddy within the Tasman EKE Box (Figures 2d and 2e), whereas the separation latitude

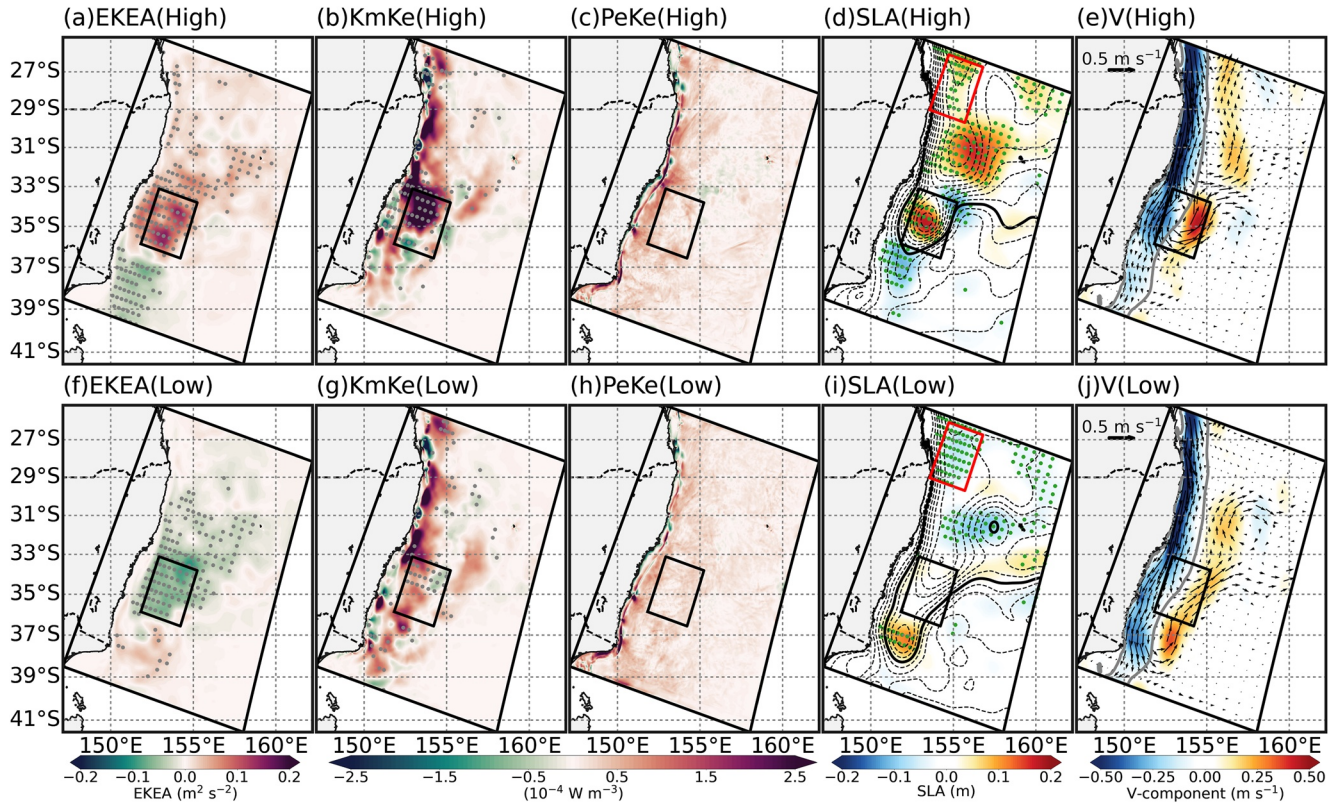

Figure 2. Composites during the high-eddy kinetic energy (EKE) periods of (a) EKE anomaly, (b) KmKe and (c) PeKe (both averaged over the upper 450 m), (d) sea level anomaly (SLA) and (e) surface along-shore velocity. The gray and green stippling in (a, b and d) indicates significance at 95% confidence interval obtained from a Monte Carlo simulation. (f–j) Composites as per (a–e), but for the low-EKE periods. Dashed lines in (d) and (i) indicate the composite sea surface height (SSH) with 0.3 m SSH contour highlighted (black line), and the red boxes denote the region used to average the upstream SLA in Figures 3b and 3c and Section 3.3. Gray lines in (e) and (j) indicate the −0.05 m s^{-1} contour of mean surface along-shore velocity. The black boxes in each panel show the Tasman EKE box.

shifts southward by ~2° during the low-EKE periods with an anticyclonic eddy south of the Tasman EKE Box (Figures 2i and 2j).

It is noteworthy that negative KmKe values occur in two small regions north of each high KmKe band (Figures 2b, 2g and S5a). The first is at ~27°S–28°S, and the second is at ~30.5°S–31.5°S. These regions are sites where frontal eddies are observed (small cyclonic eddies on the landward side of the WBC jet) (Roughan et al., 2017). Regions of negative barotropic conversion are regions of eddy decay (Gula et al., 2015). Following the Orr mechanism (Orr, 1907), eddies become tilted with the increasing background shear, and the decay of cyclonic eddies may return energy and momentum to the mean flow. The observations from HF radar measurements show that cyclonic eddies occur all year long between 30°S and 30.7°S (Mantovanelli et al., 2017; Schaeffer et al., 2017). Negative KmKe in this region indicates that the decay of cyclonic eddies converts EKE back into MKE.

Compared to KmKe, the energy conversion term PeKe through baroclinic instabilities is an order of magnitude smaller (Figures S5a and S5d), and its impact is constrained near the shelf. Despite the relatively small amplitude of PeKe, we find that positive PeKe is stronger north of the Tasman EKE Box in the high-EKE periods (Figures 2c and S5e) than in the low-EKE periods (Figures 2h and S5f), suggesting that more energy is transferred from EPE to EKE in the high-EKE periods. Furthermore, negative PeKe is observed at the same location as the first negative KmKe region (~27°S–28°S), indicating the energy conversion from EKE to EPE.

In order to understand the mechanism responsible for the EKE's interannual modulation in the Tasman EKE Box, we examine the composite SLA (Figures 2d and 2h) in the high-EKE and low-EKE periods. When the EAC jet separates from the coast and flows east, positive KmKe increases the energy conversion from

MKE to EKE and the growth of velocity anomalies, leading to the shedding of an anticyclonic eddy. During the high-EKE periods, strong positive KmKe (Figure 2b) and an anticyclonic anomaly (Figures S6a and S6c) occur in the Tasman EKE Box, indicating the formation of eddies. An anticyclonic eddy structure with positive SLA anomalies dominates the Tasman EKE Box (Figure 2d), accounting for the large amplitude high EKE anomalies. In the low-EKE periods, no significant SLA anomalies occur in the Tasman EKE Box (Figure 2i). The EAC jet is less unstable, with small velocity anomalies around these latitudes (Figures S6b and S6d). Although the perturbations are growing in every region with positive KmKe, they have not yet reached an amplitude sufficient to dominate the mean flow and pinch off as eddies in the Tasman EKE Box (Figure 2g), and the mean flow continues poleward. Compared to the high-EKE periods, the EAC jet separates further south to ~38.5°S (Figures 2i and 2j), resulting in a strong anticyclonic anomaly south of the Tasman EKE Box (Figures S6b and S6d). When the EAC separates from the coast, positive KmKe around this region allows eddies to drain energy and shed from the mean flow. Therefore, we can find an anticyclonic eddy structure with positive SLA anomalies south of the Tasman EKE Box (Figure 2i).

3.3. Predictability of Downstream EKE

Following the approach in Kerry and Roughan (2020), we compute the EAC poleward transport over the cross-sectional area inside the -0.05 m s^{-1} contour in the alongshore velocity mean. Over the 22-year simulation, we find opposing transport trends in the upstream and downstream EAC. Upstream the transport has decreased at a rate of -0.29 ± 0.21 Sv per year at 28 °S, and downstream the transport has increased at a rate of 0.82 ± 0.45 Sv per year at 36.4°S (Figure 3a). Sloyan and O'Kane (2015) indicated that the increased South Pacific gyre results in a decrease in the southward EAC transport at 25°S, and Ridgway (2007) found that the southward shift of the South Pacific subtropical gyre may lead to a stronger EAC southern extension. Our results are consistent with these studies, implying that the negative trend at 28°S and positive trend at 36.4°S are associated with the intensified South Pacific subtropical gyre that has shifted poleward.

The transport upstream is connected with downstream eddy shedding events (Kerry & Roughan, 2020). Stronger transport at 28°S enhances the downstream energy conversion from MKE to EKE through barotropic instabilities, driving anticyclonic eddies to shed from the EAC jet in the latitudinal range of 33.1°S–36.5°S. Therefore, transport at 28°S can be used as a good proxy to represent the EAC jet's upstream conditions and its impact on the downstream eddy activity. To investigate the relationship between the interannual variability of downstream EKE with upstream transport, we use the transport at 28°S to examine its correlations with the EKE in the Tasman EKE Box. The lead-lag correlations between the transport and EKE show that the transport leads EKE by 105 days with a positive correlation coefficient of 0.57 (Figure 3b, 95% significance level). The time series of 105 days lagged EKE varies in phase with transport at 28°S (Figure 3c). This timescale is consistent with the previous study by Zilberman et al. (2018) that indicated that water crossing the transect at 28°S can arrive at 33°S within 4 months. The lead time of 105 days is also similar to a prediction timescale in the Agulhas Current system. The southward Agulhas Current volume transport in the upper 500 m across 31°S leads the downstream EKE in the Agulhas Return Current region by about 4 months (Zhu et al., 2018). Our result further verifies the previous viewpoint that there is a statistically significant relationship between upstream transport and downstream eddy activity.

Furthermore, we examined the relationship between the time series of upstream SLA and downstream EKE (Figure 3b) and found a correlation coefficient of 0.58 (95% significance level) when SLA leads EKE by 77 days. SLA is a useful predictor as it is easier to measure than transport. A Monte Carlo simulation is used to test the significance of these lead-lag correlations (Text S3). We found a lead time of 93–118 days between transport and EKE at 95% confidence level and a lead time of 62–92 days between SLA and EKE (Figure 3b). Transport was computed over the cross-sectional area inside the -0.05 m s^{-1} contour of mean alongshore velocity at 28°S, and SLA was averaged between ~27°S–29°S. The lag times differ as SLA averaged over the chosen box is not directly related to alongshore transport (which is associated with the sea surface height gradient by geostrophy). We show that SLA and transport have a zero time-lag correlation of 0.82 between the two 1-year low-pass filtered time series (95% significance level). Our results show that both the transport at 28°S and the upstream SLA can potentially be used to predict the EKE in the Tasman EKE Box. A strong transport at 28°S associated with high SLA at ~27°S–29°S results in an increase in EKE in the Tasman EKE Box, and the inverse is true for a weak transport at 28°S (Figure 3d).

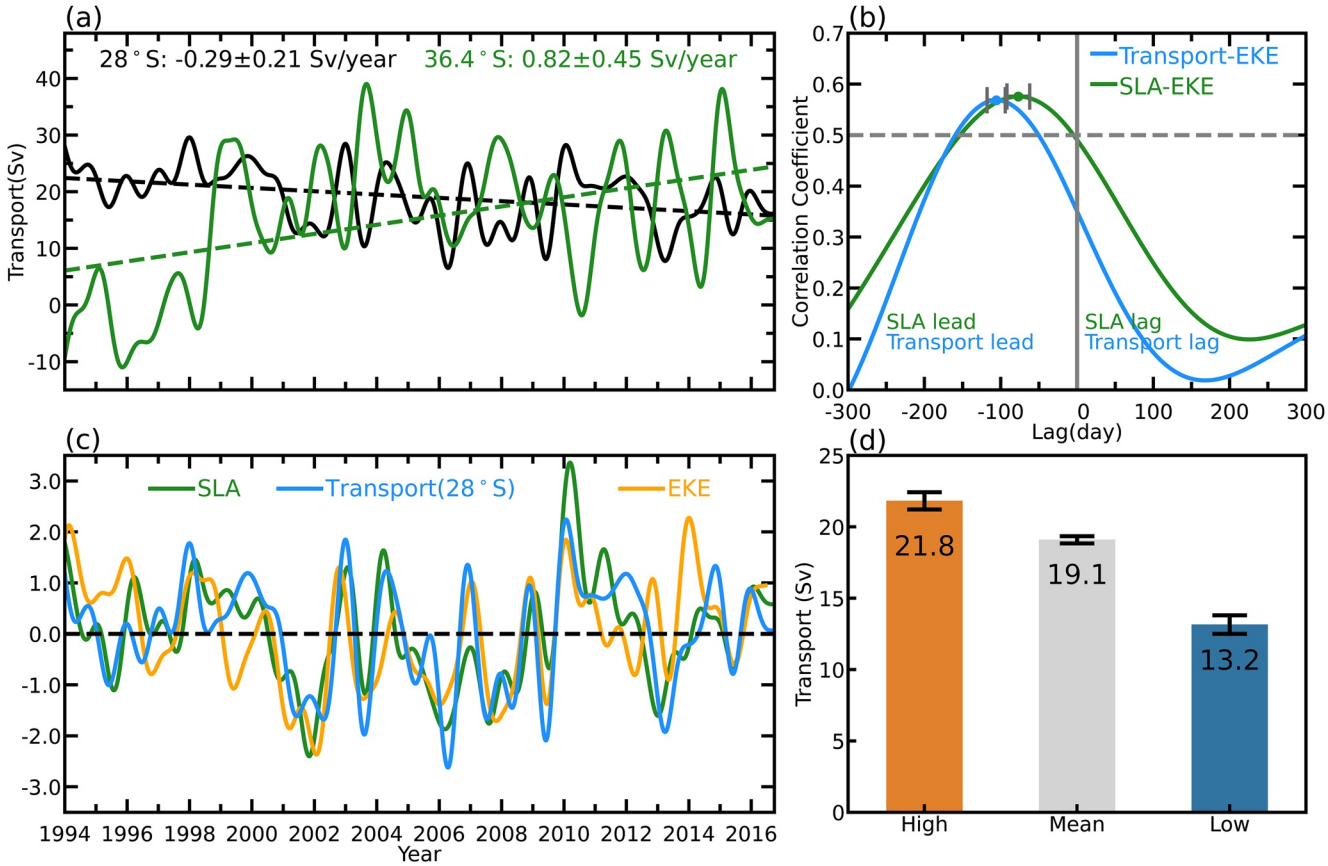

Figure 3. (a) Time series of the 1-year low-pass filtered transport at 28°S (solid black line) and 36.4°S (solid green line) with errors estimated at 95% significance level. The dashed lines indicate the linear trends of each time series. (b) Lead-lag correlations between the time series of the 1-year low-pass filtered transport and eddy kinetic energy (EKE) (blue line), sea level anomaly (SLA) and EKE (green line). Error bars indicate significance at 95% confidence interval obtained from the Monte Carlo simulation. A negative (positive) lag represents the transport or SLA leads (lags). (c) Time series of the 1-year low-pass filtered SLA averaged in the red box in Figures 2d and 2i (green line), transport at 28°S (blue line) and 105 days lagged EKE (orange line), where the time series are normalized by their respective Standard Deviation with the linear trends removed. (d) Lagged composite transports at 28°S from −105 days for the high-EKE periods (orange), the whole 22-year period (gray) and low-EKE periods (blue) at 28°S. Error bars represent 95% confidence intervals.

4. Discussion and Conclusions

Previous energetic analyses show that the contributions of barotropic and baroclinic instabilities vary in WBCs. Both barotropic and baroclinic instabilities contribute to the energy conversion from the mean flow to the eddy field in the Gulf Stream (Kang & Curchitser, 2015) and the Kuroshio Current (Yan et al., 2019). In the southern hemisphere, the Brazil Current is baroclinically unstable (Brum et al., 2017; Magalhães et al., 2017), whereas barotropic instability is the primary energy conversion term in the Agulhas Current (Elipot & Beal, 2015; Zhu et al., 2018). Despite the EAC jet having a weaker mean flow and transport, the energetic eddy field is comparable with the other large WBCs (Rykova et al., 2017). Our results show that the barotropic instabilities are the primary sources of EKE, consistent with Bowen et al. (2005), and that baroclinic instabilities are one order of magnitude smaller.

Interannual modulation of EKE by the upstream transport has been investigated in other WBCs. Sun et al. (2016) indicated that the strengthened Kuroshio intrusion enhances the baroclinic instability and leads to high EKE in the northeastern South China Sea. Zhu et al. (2018) found that the upstream Agulhas Current inflow variability regulates downstream interannual EKE fluctuations in the Agulhas Return Current region. Our results show that the interannual variability of EKE in the Tasman EKE Box is modulated by the transport at 28°S. We suggest that this mechanism can potentially be used to investigate the downstream interannual EKE variability in other WBCs, such as the Brazil Current and Gulf Stream.

Anticyclonic eddies form when the EAC separates from the coast with large velocity perturbations (high KmKe). We find that the EAC jet separates at different latitudes during high-EKE (more northern separation) and low-EKE periods (more southern separation). Therefore, the variability in EAC separation latitude may influence the variability of EKE in the Tasman EKE Box. In contrast to other WBCs, the EAC separates within a broad latitudinal range. Earlier studies suggested that EAC separation may be affected by westward propagating Rossby waves (Godfrey et al., 1980; Marchesiello & Middleton, 2000). Hence we suggest it is worth investigating the influence of Rossby waves on the variability in EKE in the Tasman EKE Box in the future.

Cyclonic eddies are known to be more productive due to the persistent upwelling of nutrient-rich water in their core. Within the so-called 'Eddy Avenue', which encompasses our Tasman EKE Box, the average chlorophyll-a concentration for cyclonic eddies is double that of anticyclonic eddies and 16% higher than those in the rest of the Tasman Sea (Everett et al., 2012). Roughan et al. (2017) found that a frontal eddy is significantly more productive than a mesoscale cyclone, despite its small size and short life. Based on the energetic analysis, we find negative KmKe values associated with the decay of cyclonic eddies occurs at ~27°S–28°S and ~30.5°S–31.5°S, consistent with the existence of frontal eddies in these locations with likely higher productivity.

This study is the first to use a long-term (22-year), high-resolution (<6 km) ocean model simulation to investigate the energetics of eddy-mean flow interactions in the EAC system. We find strong interannual variability in EKE in the Tasman EKE Box, with large amplitude anomalies dominate 15.3% and 18.1% of the time for high and low EKE anomalies, respectively. Barotropic instabilities dominate the energy conversion in the EAC system, with a much higher KmKe in the high-EKE periods, playing an important role in eddy formation. We show energy conversion from EKE back to MKE around ~27°S–28°S and ~30.5°S–31.5°S, inshore of the EAC jet consistent with the decay of cyclonic eddies at these latitudes. Anticyclonic eddy structures are observed in the Tasman EKE Box in the high-EKE periods, but they penetrate further south by ~2° in the low-EKE periods. The 1-year low-pass filtered time series of EKE in the Tasman EKE Box is significantly correlated with transport at 28°S ($R = 0.57$) and upstream SLA at ~27°S–29°S ($R = 0.58$). Therefore, both the upstream transport and SLA can be used as indices to predict downstream EKE. Our results provide new insights into predicting the interannual modulation of EKE in the Tasman EKE Box and shed light on the mechanisms of eddy-mean flow interactions in the EAC system.

Data Availability Statement

Model initial and boundary conditions are provided by CSIRO Australia BRAN2016 and available at https://research.csiro.au/bluelink/outputs/data-access/. The atmospheric forcing BARRA-R data are obtained from http://www.bom.gov.au/research/projects/reanalysis/. The tide forcing is obtained from https://www.tpxo.net/global/tpxo8-atlas. The AVISO products are downloaded from https://resources.marine.copernicus.eu/?option=com_csw&view=details&product_id=SEALEVEL_GLO_PHY_L4_REP_OBSERVATIONS_008_047. The model output (https://doi.org/10.26190/TT1Q-NP46 [Li et al., 2021]) is available at https://researchdata.edu.au/high-resolution-22-version-20/1676421. This research also includes computations using the computational cluster doi.org/Katana (2010) https://doi.org/10.26190/669X-A286, supported by Research Technology Services at UNSW Sydney.

Acknowledgments
This research was partially supported by the Australian Research Council grants DP140102337, LP160100162, LP170100498. This research was undertaken with the assistance of resources and services from the National Computational Infrastructure (NCI), which is supported by the Australian Government.

References

Bowen, M. M., Wilkin, J. L., & Emery, W. J. (2005). Variability and forcing of the East Australian Current. *Journal of Geophysical Research*, *110*, C03019. https://doi.org/10.1029/2004JC002533

Brum, A. L., de, Azevedo, J. L. L., de, Oliveira, L. R., & Calil, P. H. R. (2017). Energetics of the Brazil Current in the Rio Grande Cone region. *Deep-Sea Research Part I: Oceanographic Research Papers*, *128*, 67–81. https://doi.org/10.1016/j.dsr.2017.08.014

Bull, C. Y., Kiss, A. E., Jourdain, N. C., England, M. H., & van, Sebille, E. (2017). Wind forced variability in eddy formation, eddy shedding, and the separation of the East Australian Current. *Journal of Geophysical Research: Oceans*, *122*, 9980–9998. https://doi.org/10.1002/2017JC013311

Cetina-Heredia, P., Roughan, M., Liggins, G., Coleman, M. A., & Jeffs, A. (2019). Mesoscale circulation determines broad spatio-temporal settlement patterns of lobster. *PloS One*, *14*(2), e0211722. https://doi.org/10.1371/journal.pone.0211722

Cetina-Heredia, P., Roughan, M., Sebille, E. V., & Coleman, M. A. (2014). Long-term trends in the East Australian Current separation latitude and eddy driven transport. *Journal of Geophysical Research: Oceans*, *119*, 4351–4366. https://doi.org/10.1002/2014JC010071

Chassignet, E. P., & Xu, X. (2017). Impact of horizontal resolution (1/12° to 1/50°) on Gulf Stream separation, penetration, and variability. *Journal of Physical Oceanography*, *47*(8), 1999–2021. https://doi.org/10.1175/JPO-D-17-0031.1
Chen, R., Flierl, G. R., & Wunsch, C. (2014). A description of local and nonlocal eddy-mean flow interaction in a global eddy-permitting state estimate. *Journal of Physical Oceanography*, *44*(9), 2336–2352. https://doi.org/10.1175/JPO-D-14-0009.1
Ducet, N., Le Traon, P. Y., & Reverdin, G. (2000). Global high-resolution mapping of ocean circulation from TOPEX/Poseidon and ERS-1 and -2. *Journal of Geophysical Research*, *105*(C8), 19477–19498. https://doi.org/10.1029/2000JC900063
Egbert, G. D., & Erofeeva, S. Y. (2002). Efficient inverse modeling of Barotropic Ocean Tides. *Journal of Atmospheric and Oceanic Technology*, *19*(2), 183–204. https://doi.org/10.1175/1520-0426(2002)019<0183:eimobo>2.0.co;2
Elipot, S., & Beal, L. M. (2015). Characteristics, energetics, and origins of Agulhas Current Meanders and their limited influence on ring shedding. *Journal of Physical Oceanography*, *45*(9), 2294–2314. https://doi.org/10.1175/JPO-D-14-0254.1
Everett, J. D., Baird, M. E., Oke, P. R., & Suthers, I. M. (2012). An avenue of eddies: Quantifying the biophysical properties of mesoscale eddies in the Tasman Sea. *Geophysical Research Letters*, *39*(16), L16608. https://doi.org/10.1029/2012GL053091
Godfrey, J. S. (1989). A Sverdrup model of the depth-integrated flow for the world ocean allowing for island circulations. *Geophysical & Astrophysical Fluid Dynamics*, *45*(1–2), 89–112. https://doi.org/10.1080/03091928908208894
Godfrey, J. S., Cresswell, G. R., Golding, T. J., Pearce, A. F., & Boyd, R. (1980). The separation of the East Australian Current. *Journal of Physical Oceanography*, *10*(3), 430–440. https://doi.org/10.1175/1520-0485(1980)010<0430:tsotea>2.0.co;2
Greatbatch, R. J., Zhai, X., Claus, M., Czeschel, L., & Rath, W. (2010). Transport driven by eddy momentum fluxes in the Gulf Stream Extension region. *Geophysical Research Letters*, *37*(24), L24401. https://doi.org/10.1029/2010GL045473
Gula, J., Molemaker, M. J., & McWilliams, J. C. (2015). Gulf Stream Dynamics along the Southeastern U.S. Seaboard. *Journal of Physical Oceanography*, *45*(3), 690–715. https://doi.org/10.1175/JPO-D-14-0154.1
Halo, I., Penven, P., Backeberg, B., Ansorge, I., Shillington, F., & Roman, R. (2014). Mesoscale eddy variability in the southern extension of the East Madagascar Current: Seasonal cycle, energy conversion terms, and eddy mean properties. *Journal of Geophysical Research: Oceans*, *119*(10), 7324–7356. https://doi.org/10.1002/2014JC009820
Kang, D., & Curchitser, E. N. (2015). Energetics of eddy-mean flow interactions in the Gulf Stream Region. *Journal of Physical Oceanography*, *45*(4), 1103–1120. https://doi.org/10.1175/JPO-D-14-0200.1
Kerry, C., Powell, B., Roughan, M., & Oke, P. (2016). Development and evaluation of a high-resolution reanalysis of the East Australian Current region using the Regional Ocean Modelling System (ROMS 3.4) and Incremental Strong-Constraint 4-Dimensional Variational (IS4D-Var) data assimilation. *Geoscientific Model Development*, *9*(10), 3779–3801. https://doi.org/10.5194/gmd-9-3779-2016
Kerry, C., & Roughan, M. (2020). Downstream evolution of the East Australian Current System: Mean flow, seasonal, and intra-annual variability. *Journal of Geophysical Research: Oceans*, *125*(5). https://doi.org/10.1029/2019JC015227
Kerry, C., Roughan, M., & Powell, B. (2018). Observation impact in a regional reanalysis of the East Australian Current System. *Journal of Geophysical Research: Oceans*, *123*(10), 7511–7528. https://doi.org/10.1029/2017JC013685
Kuo, Y. C., & Chern, C. S. (2011). Numerical study on the interactions between a mesoscale eddy and a Western Boundary Current. *Journal of Oceanography*, *67*(3), 263–272. https://doi.org/10.1007/s10872-011-0026-3
Li, J., Kerry, C., & Roughan, M. (2021). A high-resolution, 22-year, free-running, hydrodynamic simulation of the East Australia Current System using the Regional Ocean Modeling System (Version 2.0). *UNSW Dataset*. https://doi.org/10.26190/TT1Q-NP46
Macdonald, H., Roughan, M., Baird, M., & Wilkin, J. (2016). The formation of a cold-core eddy in the East Australian Current. *Continental Shelf Research*, *114*, 72–84. https://doi.org/10.1016/j.csr.2016.01.002
Magalhães, F. C., Azevedo, J. L. L., & Oliveira, L. R. (2017). Energetics of eddy-mean flow interactions in the Brazil current between 20°S and 36°S. *Journal of Geophysical Research: Oceans*, *122*(8), 6129–6146. https://doi.org/10.1002/2016JC012609
Malan, N., Archer, M., Roughan, M., Cetina-Heredia, P., Hemming, M., Rocha, C., et al. (2020). Eddy-driven cross-shelf transport in the East Australian Current separation zone. *Journal of Geophysical Research: Oceans*, *125*(2). https://doi.org/10.1029/2019JC015613
Maltrud, M. E., & McClean, J. L. (2005). An eddy resolving global 1/10°ocean simulation. *Ocean Modelling*, *8*(1), 31–54. https://doi.org/10.1016/j.ocemod.2003.12.001
Mantovanelli, A., Keating, S., Wyatt, L. R., Roughan, M., & Schaeffer, A. (2017). Lagrangian and Eulerian characterization of two counter-rotating submesoscale eddies in a Western Boundary Current. *Journal of Geophysical Research: Oceans*, *122*(6), 4902–4921. https://doi.org/10.1002/2016JC011968
Marchesiello, P., & Middleton, J. H. (2000). Modeling the East Australian Current in the Western Tasman Sea. *Journal of Physical Oceanography*, *30*(11), 2956–2971. https://doi.org/10.1175/1520-0485(2001)031<2956:mteaci>2.0.co;2
Mata, M. M., Tomczak, M., Wijffels, S., & Church, J. A. (2000). East Australian Current volume transports at 30°S: Estimates from the World Ocean Circulation Experiment hydrographic sections PR11/P6 and the PCM3 current meter array. *Journal of Geophysical Research: Oceans*, *105*(C12), 28509–28526. https://doi.org/10.1029/1999jc000121
Mata, M. M., Wijffels, S. E., Church, J. A., & Tomczak, M. (2006). Eddy shedding and energy conversions in the East Australian Current. *Journal of Geophysical Research: Oceans*, *111*, C09034. https://doi.org/10.1029/2006JC003592
Nonaka, M., Sasaki, H., Taguchi, B., & Schneider, N. (2020). Atmospheric-driven and intrinsic interannual-to-decadal variability in the Kuroshio Extension Jet and Eddy Activities. *Frontiers in Marine Science*, *7*, 805. https://doi.org/10.3389/fmars.2020.547442
Oke, P. R., Roughan, M., Cetina-Heredia, P., Pilo, G. S., Ridgway, K. R., Rykova, T., et al. (2019). Revisiting the circulation of the East Australian Current: Its path, separation, and eddy field. *Progress in Oceanography*, *176*, 102139. https://doi.org/10.1016/j.pocean.2019.102139
Oliver, E. C. J., O'Kane, T. J., & Holbrook, N. J. (2015). Projected changes to Tasman Sea eddies in a future climate. *Journal of Geophysical Research: Oceans*, *120*(11), 7150–7165. https://doi.org/10.1002/2015JC010993
Orr, W. M. (1907). The stability or instability of the steady motions of a perfect liquid and of a viscous liquid. Part II: A Viscous Liquid. *Proceedings of the Royal Irish Academy - Section A: Mathematical and Physical Sciences*, *27*, 69–138.
Qiu, B., & Chen, S. (2004). Seasonal modulations in the eddy field of the South Pacific Ocean. *Journal of Physical Oceanography*, *34*(7), 1515–1527. https://doi.org/10.1175/1520-0485(2004)034<1515:smitef>2.0.co;2
Qiu, B., Chen, S., Klein, P., Sasaki, H., & Sasai, Y. (2014). Seasonal mesoscale and submesoscale eddy variability along the North Pacific subtropical countercurrent. *Journal of Physical Oceanography*, *44*(12), 3079–3098. https://doi.org/10.1175/JPO-D-14-0071.1
Ribbat, N., Roughan, M., Powell, B., Rao, S., & Kerry, C. G. (2020). Transport variability over the Hawkesbury Shelf (31.5–34.5°S) driven by the East Australian Current. *PloS One*, *15*(11), 1–27. https://doi.org/10.1371/journal.pone.0241622
Ridgway, K. R. (2007). Long-term trend and decadal variability of the southward penetration of the East Australian Current. *Geophysical Research Letters*, *34*(13), L13613. https://doi.org/10.1029/2007GL030393

Ridgway, K. R., Coleman, R. C., Bailey, R. J., & Sutton, P. (2008). Decadal variability of East Australian Current transport inferred from repeated high-density XBT transects, a CTD survey and satellite altimetry. *Journal of Geophysical Research: Oceans*, *113*(C8), C08039. https://doi.org/10.1029/2007JC004664

Roughan, M., Keating, S. R., Schaeffer, A., Cetina Heredia, P., Rocha, C., Griffin, D., et al. (2017). A tale of two eddies: The biophysical characteristics of two contrasting cyclonic eddies in the East Australian Current System. *Journal of Geophysical Research: Oceans*, *122*(3), 2494–2518. https://doi.org/10.1002/2016JC012241

Rykova, T., Oke, P. R., & Griffin, D. A. (2017). A comparison of the structure, properties, and water mass composition of quasi-isotropic eddies in Western Boundary Currents in an eddy-resolving ocean model. *Ocean Modelling*, *114*, 1–13. https://doi.org/10.1016/j.ocemod.2017.03.013

Schaeffer, A., Gramoulle, A., Roughan, M., & Mantovanelli, A. (2017). Characterizing frontal eddies along the East Australian Current from HF radar observations. *Journal of Geophysical Research: Oceans*, *122*(5), 3964–3980. https://doi.org/10.1002/2016JC012171

Schubert, R., Biastoch, A., Cronin, M. F., & Greatbatch, R. J. (2018). Instability-driven Benthic Storms below the Separated Gulf Stream and the North Atlantic Current in a High-Resolution Ocean Model. *Journal of Physical Oceanography*, *48*(10), 2283–2303. https://doi.org/10.1175/JPO-D-17-0261.1

Sloyan, B. M., & O'Kane, T. J. (2015). Drivers of decadal variability in the Tasman Sea. *Journal of Geophysical Research: Oceans*, *120*(5), 3193–3210. https://doi.org/10.1002/2014JC010550

Sloyan, B. M., Ridgway, K. R., & Cowley, R. (2016). The East Australian Current and property transport at 27°S from 2012 to 2013. *Journal of Physical Oceanography*, *46*(3), 993–1008. https://doi.org/10.1175/JPO-D-15-0052.1

Storch, J.-S. V., Eden, C., Fast, I., Haak, H., Hernández-Deckers, D., Maier-Reimer, E., et al. (2012). An estimate of the Lorenz Energy Cycle for the world ocean based on the 1/10° STORM/NCEP Simulation. *Journal of Physical Oceanography*, *42*(12), 2185–2205. https://doi.org/10.1175/JPO-D-12-079.1

Su, C.-H., Eizenberg, N., Steinle, P., Jakob, D., Fox-Hughes, P., White, C. J., et al. (2019). BARRA v1.0: The bureau of meteorology atmospheric high-resolution regional reanalysis for Australia. *Geoscientific Model Development*, *12*(5), 2049–2068. https://doi.org/10.5194/gmd-12-2049-2019

Sun, Z., Zhang, Z., Zhao, W., & Tian, J. (2016). Interannual modulation of eddy kinetic energy in the northeastern South China Sea as revealed by an eddy-resolving OGCM. *Journal of Geophysical Research: Oceans*, *121*(5), 3190–3201. https://doi.org/10.1002/2015JC011497

Yan, X., Kang, D., Curchitser, E. N., & Pang, C. (2019). Energetics of eddy-mean flow interactions along the Western Boundary Currents in the North Pacific. *Journal of Physical Oceanography*, *49*(3), 789–810. https://doi.org/10.1175/JPO-D-18-0201.1

Yang, Y., & Liang, X. S. (2016). The Instabilities and multiscale energetics underlying the mean-interannual-eddy interactions in the Kuroshio Extension Region. *Journal of Physical Oceanography*, *46*(5), 1477–1494. https://doi.org/10.1175/JPO-D-15-0226.1

Yang, Y., & Liang, X. S. (2018). On the seasonal eddy variability in the Kuroshio Extension. *Journal of Physical Oceanography*, *48*(8), 1675–1689. https://doi.org/10.1175/JPO-D-18-0058.1

Ypma, S. L., Sebille, E. V., Kiss, A. E., & Spence, P. (2016). The separation of the East Australian Current: A Lagrangian approach to potential vorticity and upstream control. *Journal of Geophysical Research: Oceans*, *121*(1), 758–774. https://doi.org/10.1002/2015JC011133

Zhu, Y., Qiu, B., Lin, X., & Wang, F. (2018). Interannual eddy kinetic energy modulations in the Agulhas Return Current. *Journal of Geophysical Research: Oceans*, *123*(9), 6449–6462. https://doi.org/10.1029/2018JC014333

Zilberman, N. V., Roemmich, D. H., Gille, S. T., & Gilson, J. (2018). Estimating the velocity and transport of Western Boundary Current Systems: A case study of the East Australian Current near Brisbane. *Journal of Atmospheric and Oceanic Technology*, *35*(6), 1313–1329. https://doi.org/10.1175/JTECH-D-17-0153.1